

This is the accepted manuscript made available via CHORUS. The article has been published as:

Testing the Role of Recollision in N_{2}^{+} Air Lasing

Mathew Britton, Patrick Laferrière, Dong Hyuk Ko, Zhengyan Li, Fanqi Kong, Graham Brown, Andrei Naumov, Chunmei Zhang, Ladan Arissian, and P. B. Corkum

Phys. Rev. Lett. **120**, 133208 — Published 30 March 2018

DOI: [10.1103/PhysRevLett.120.133208](https://doi.org/10.1103/PhysRevLett.120.133208)

Testing the role of recollision in N_2^+ air lasing

Mathew Britton,^{1,*} Patrick Laferrière,¹ Dong Hyuk Ko,¹ Zhengyan Li,¹ Fanqi Kong,¹ Graham Brown,¹ Andrei Naumov,² Chunmei Zhang,¹ Ladan Arissian,^{1,2,3} and P. B. Corkum^{1,2}

¹*University of Ottawa, Ottawa, Ontario, Canada*

²*National Research Council of Canada, Ottawa, Ontario, Canada*

³*University of New Mexico, Albuquerque, New Mexico, USA*

(Dated: January 22, 2018)

It has been known for many years that during filamentation of femtosecond light pulses in air, gain is observed on the B to X transition in N_2^+ . While the gain mechanism remains unclear, it has been proposed that recollision, a process that is fundamental to much of strong field science, is critical for establishing gain. We probe this hypothesis by directly comparing the influence of the ellipticity of the pump light on gain in air filaments. Then, we decouple filamentation from gain by measuring the gain in a thin gas jet that we also use for high harmonic generation. The latter allows us to compare the dependence of the gain on the ellipticity of the pump with the dependence of the high harmonic signal on the ellipticity of the fundamental. We find that gain and harmonic generation have very different behaviour in both filaments and in the jet. In fact, in a jet we even measure gain with circular polarization. Thus, we establish that recollision does not play a significant role in creating the inversion.

Light filamentation [1–3] results from the interplay between Kerr-induced self-focusing and plasma defocusing that contribute to the refractive index profile with opposite signs. The light intensity in a single filament is clamped by this balance at a value of $\sim 5 \times 10^{13} \text{ W cm}^{-2}$ independent of the input energy and beam profile [3, 4]. The filament is accompanied by a variety of emissions, with on-axis components at frequencies covering a wide range from terahertz to harmonics of the fundamental beam [3]. The directional emissions observed from the neutral nitrogen molecule [5–10] and the nitrogen molecular cation [10–17], known as “air lasing,” are of particular interest for remote sensing.

Conventional air lasing combines self-focusing of a short, high power laser pulse with optical breakdown of air molecules. As the lasing medium is pumped, the frequency of the pump beam changes, and the duration of the pump pulse varies with time in a complex manner [18–20]. In addition, the spatial profile of the pump beam is time-dependent and, if the polarization is not exactly linear, the polarization of the pump beam is also time-dependent [21, 22]. While the pumping mechanism for the gain is not yet well understood, even under these conditions, the gain on the $\text{B}^2\Sigma_u^+$ to $\text{X}^2\Sigma_g^+$ transitions in N_2^+ seems to be reproducible. Thus, multiphoton ionization provides a robust, probably general pumping mechanism that is important to understand.

Recollision is one of the most unique characteristics of multiphoton ionization and it is known to be important in N_2 double ionization [24, 25]. The large inelastic scattering cross section of low energy electrons leading to transitions from $\text{X}^2\Sigma_g^+$ to $\text{B}^2\Sigma_u^+$ in N_2^+ [23] has led to suggestions that recollision could play a role in creating the inversion. In this proposed mechanism, gain is created by recolliding electrons that excite the parent ion [15].

We begin by applying a semi-classical recollision model

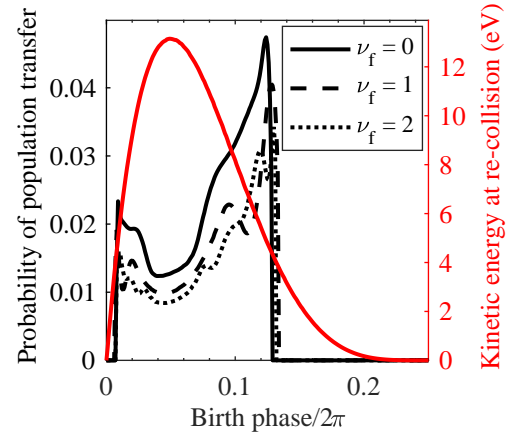


FIG. 1. Population transfer from $\text{X}^2\Sigma_g^+(\nu_i = 0)$ to $\text{B}^2\Sigma_u^+(\nu_f = 0, 1, 2)$ in N_2^+ via recollision using linear polarization at 800 nm and $7 \times 10^{13} \text{ W cm}^{-2}$. The kinetic energy at the time of recollision (also shown) is calculated using the classical electron trajectories and the electron wave function expansion is estimated in the absence of the Coulomb potential. Inelastic scattering cross sections [23] are used to calculate the population transfer.

often used in strong field calculations, together with published excitation cross sections [23], to predict the role of recollision in transferring population to the vibrational states of the $\text{B}^2\Sigma_u^+$ state of N_2^+ . Then we experimentally determine the ellipticity dependence of gain on the $\text{B}^2\Sigma_u^+(\nu = 0)$ to $\text{X}^2\Sigma_g^+(\nu = 1)$ transition at 428 nm during filamentation in room air, using the near 428 nm continuum generated in the filament as a seed pulse. While the gain disappears for circular polarization, significant gain remains until very near circular. Next, we eliminate the complexity of the filament by producing gain in the same gas jet that we use for high-harmonic genera-

tion. This enables us to directly compare the ellipticity of the high harmonics in N_2 with the gain on the $B^2\Sigma_u^+$ to $X^2\Sigma_g^+$ transitions in N_2^+ . Even under these highly controlled conditions, we do not find any evidence of sharp ellipticity dependence of the gain that characterizes other recollision events.

To set the stage for our measurements, we confirm the contribution of recollision to gain by following classical recollision trajectories while ignoring the Coulomb field [26]. The kinetic energy at the time of recollision is shown in Figure 1 as a function of birth phase using a wavelength of 800 nm and intensity of $7 \times 10^{13} \text{ W cm}^{-2}$. Figure 1 also shows the population transfer from $N_2^+ X^2\Sigma_g^+(\nu_i = 0)$ to $B^2\Sigma_u^+(\nu_f = 0, 1, 2)$ from recollision determined using the energy-dependent cross section and electron wave function spread. The $X^2\Sigma_g^+$ to $B^2\Sigma_u^+$ population transfer is 2.8% for the conditions in Figure 1, with $\sim 1\%$ of the population that was initially in the $X^2\Sigma_g^+$ state transferred to $\nu_f = 0$ of the $B^2\Sigma_u^+$ state. The total population transfer increases to $\sim 4\%$ by $10^{15} \text{ W cm}^{-2}$.

While this model can accurately predict the ellipticity dependence of recollision events such as non-sequential double ionization and high harmonic generation [27], it does not yield a quantitative prediction of double ionization since Coulomb focusing and high order returns are not included. These effects enhance correlated double ionization in He^+/He^{2+} by a factor of ~ 5 [28, 29] and we might expect it to yield a similar enhancement to the N_2^+ gain. Therefore, these results suggest that recollision can participate in establishing gain, although it is unlikely to be the dominant mechanism.

To search for evidence of recollision experimentally, we follow the common strong field procedure of adding ellipticity to the generating laser. Elliptically polarized light prevents electron trajectories from returning to the parent ion, which greatly reduces the overlap of the spreading electron wave function and the ion, thereby removing the contribution of recollision. We first measure the ellipticity dependence of the gain in atmospheric air and expand on previous experiments [10, 13, 15, 30]. As depicted in Figure 2(a) for the unfocused beam, a quarter wave plate is used to control the ellipticity of a femtosecond laser (800 nm, $\sim 25 \text{ fs}$, $\sim 3.3 \text{ mJ}$), while a polarizer is used to determine the polarization state. A measurement of the unfocused beam is presented in Figure 2(c). The colour scale is the normalized transmission of the 800 nm beam through the polarizer. The ellipticity is deduced from the data in each horizontal row using the Jones matrix representation of polarization [31]. The zero point on the vertical and horizontal axes corresponds to the creation and transmission of horizontal polarization, respectively.

To study the gain, we add a 30 cm focal length lens after the quarter wave plate to focus the beam in ambient air and create a plasma channel. The resulting

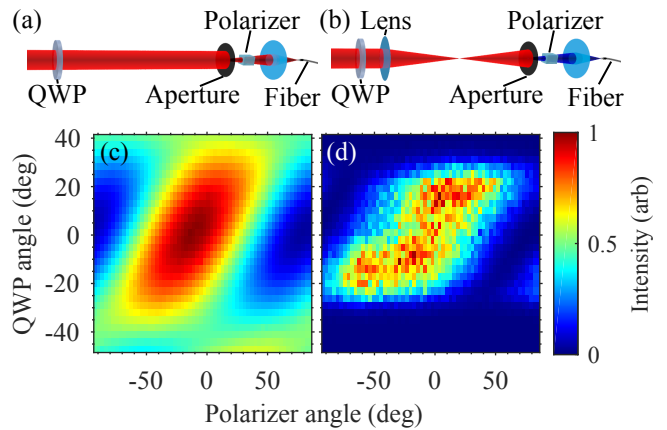


FIG. 2. (a) Experimental diagram of calibration measurement in air. (b) Experimental diagram of gain measurement in air. (c) Normalized transmission intensity (colour scale) of the unfocused 800 nm beam as a function of quarter wave plate (QWP) and polarizer angle in degrees. (d) Intensity of 428 nm emission (colour scale) from air filament as a function of QWP and polarizer angle in degrees.

plasma emission is typically accompanied with a continuum generated from self-phase modulation and pulse self-steepening in addition to molecular emissions. The continuum that overlaps the gain lines serves as a probe. The conical emissions terminate on an aperture, and the center of the beam travels through the polarizer. A fiber spectrometer with $\sim 0.4 \text{ nm}$ resolution analyzes the transmitted light. Figure 2(b) shows a diagram of this experiment. We observe emissions from $N_2^+ B^2\Sigma_u^+$ to $X^2\Sigma_g^+$ for vibrational states $\nu = 0 \rightarrow \nu = 0$ (391 nm), $\nu = 0 \rightarrow \nu = 1$ (428 nm), and $\nu = 0 \rightarrow \nu = 2$ (471 nm).

We measure the polarization characteristics of the on-axis plasma emissions using the same approach as the unfocused beam. The colour scale in Figure 2(d) represents the intensity at 428 nm transmitted through the polarizer. The figure shows that there is a polarizer angle that yields no transmission for every ellipticity (QWP Angle); therefore, the emission is always linearly polarized. Furthermore, the orientation of the linearly polarized 428 nm emission follows the major axis of the ellipse of the pump beam. Note that the polarization rotates more than it did for the unfocused beam due to nonlinear polarization rotation [21, 31]. We observe identical features for the other available emission lines, but they suffer from too much (471 nm) or too little (391 nm) continuum.

Figure 2(d) also shows that the intensity is maximum with an elliptical input polarization at a quarter wave plate angle of ~ 18 degrees, which is consistent with similar observations [15, 30]. The intensity of the emission is determined by the gain and the continuum available to seed it, so it is important to consider the continuum in this context. Continuum generation strongly depends on laser ellipticity [32] and will influence the emission if the

gain is not saturated.

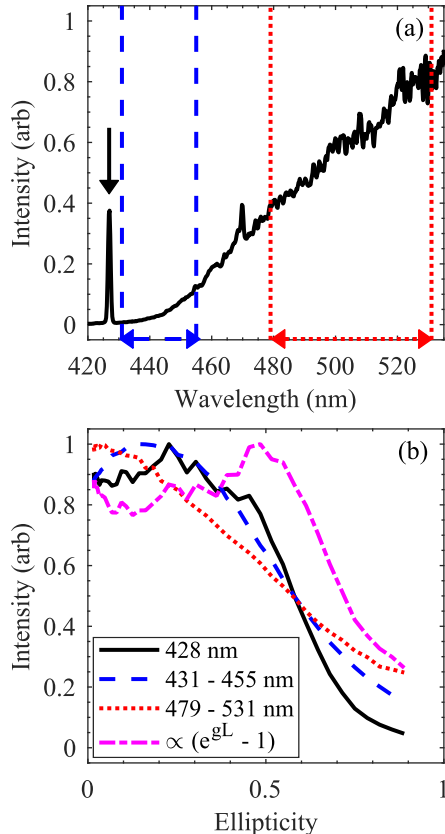


FIG. 3. (a) Spectrum of the forward emission showing continuum and ion lines at 428 nm and 471 nm. Regions of the continuum next to (431 to 455 nm) and far from (479 to 531 nm) the emission at 428 nm are highlighted using vertical lines. (b) Intensity integrated over the regions highlighted in Figure 3(a), and 428 nm intensity divided by the continuum next to the emission ($\propto e^{gL} - 1$) showing that the gain is maximum at an ellipticity of ~ 0.45 .

The continuum is highlighted in Figure 3(a), where the spectrum is separated into three regions: the ion emission at 428 nm, continuum next to the ion emission (431 - 455 nm), and continuum far from the ion emission (479 - 531 nm). The integrated intensity in these three regions is shown in Figure 3(b) as a function of the ellipticity of the unfocused beam. The 428 nm emission shows increased intensity for a nonzero ellipticity similar to Figure 2(d). The nearby continuum also shows an enhancement, but the farther continuum does not.

We assume that the continuum next to the ion emission behaves like the seed for the gain (i.e. the continuum at 428 nm that is amplified); therefore, we divide the integrated intensity at 428 nm by the nearby continuum to obtain a quantity proportional to $e^{gL} - 1$, which depends on gain g and plasma length L . It is maximum at an ellipticity of ~ 0.45 in Figure 3(b). The results for 391 nm and 471 nm show similar behaviour.

We use a range of focusing conditions (F-number = 4

to 40) to vary plasma length and formation [33], and a range of pulse widths (25 fs to 200 fs) to vary the significance of the alignment dynamics on N_2 and O_2 in the air [31]. The ellipticity at maximum gain depends on focusing geometry and pulse width but we always observe a strong gain that is enhanced for small ellipticity (0.2 - 0.5) and then falls off with increasing ellipticity. This suggests that there is a fundamental reason for the enhancement at nonzero ellipticity that is not influenced by filamentation dynamics and the mechanism of linear and nonlinear focusing [33]. Therefore, we remove the complexity of filamentation by focusing in vacuum into a narrow supersonic gas jet. This allows us to make a one-to-one comparison between the ellipticity dependence of gain and high-harmonic signal strength [27].

The pulsed gas jet has a 250 μm wide opening and a ~ 7 atmosphere backing pressure of nitrogen. The nozzle is located $\sim 200 \mu\text{m}$ upstream from the laser focus in vacuum. The pump pulse (800 nm, ~ 32 fs, ~ 2.5 mJ) creates a plasma channel in the expanding jet that is centered at the laser focus. We measure no significant spatial or spectral distortion of the pump pulse, so we use an external probe to seed the gain. The most readily available seed is second harmonic of the pump, so a weak portion of the 800 nm beam is separated, frequency-doubled, delayed, and recombined collinearly to act as a seed for the gain at 391 nm. The probe pulse is always linearly polarized and sufficiently weak to measure the small-signal gain. A half and quarter wave plate control the ellipticity and orientation of the pump beam which is calibrated near the focus. The experiment is illustrated in Figure 4(a).

The delayed probe passes through the plasma where the pump-induced gain amplifies the spectrum at 391 nm. The bandwidth of the frequency-doubled seed does not cover 428 nm, so it is not amplified. The probe beam is refocused onto the fiber spectrometer to monitor the amplification as a function of delay, which shows a rapid decay often modulated by structures centered at the quarter and half rotational revivals. It encodes information about the rotational wave packets launched by the pump in the $B^2\Sigma_u^+(\nu = 0)$ and $X^2\Sigma_g^+(\nu = 0)$ states [34]. These modulations will be the subject of a future publication and are similar to those reported in a gas cell [35, 36]. In the absence of the seed, no ion emission is measured.

Figure 4(b) shows the externally-seeded gain as a function of pump ellipticity at two delays and a pump intensity of $\sim 7 \times 10^{14} \text{ W cm}^{-2}$. Significant gain is measured for all ellipticities, even circular polarization, and there is a slight enhancement at intermediate ellipticities similar to what is observed in air.

Next we broaden the seed spectrum using self-phase modulation in fused silica to cover both 391 and 428 nm. The resulting ellipticity dependence of the normalized externally-seeded gain is shown in Figure 4(c) for both lines at a pump intensity of $\sim 4.5 \times 10^{14} \text{ W cm}^{-2}$ and a delay of ~ 0.45 ps. The gain at 428 nm is $\sim 40\%$ of the

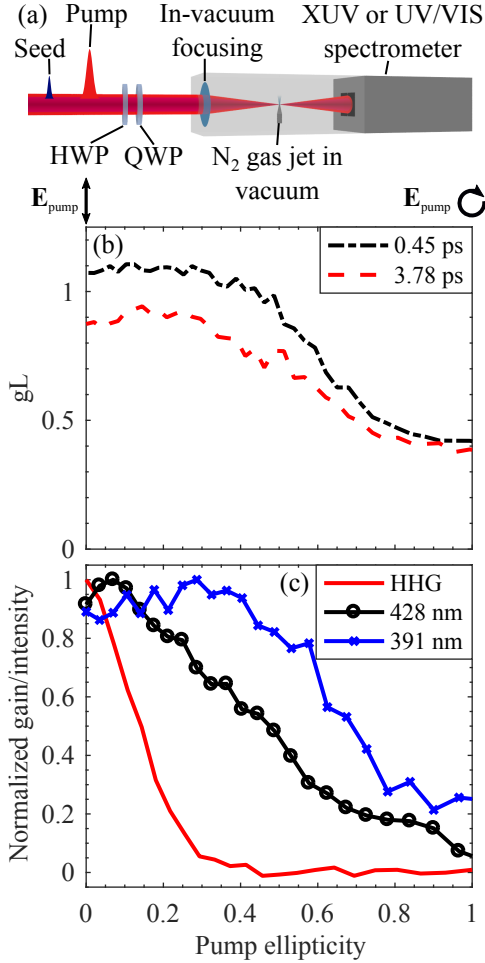


FIG. 4. (a) Experimental diagram showing the collinear pump and probe focusing into the supersonic gas jet. The pump is elliptically polarized and the seed is linearly polarized. The amplified seed is monitored on a spectrometer as a function of delay. High harmonics from the pump are measured using an XUV spectrometer. (b) Gain (gL) at 391 nm in the gas jet as a function of pump ellipticity at two seed delay times (0.45 and 3.78 ps) for a pump intensity of $\sim 7 \times 10^{14} \text{ W cm}^{-2}$. (c) Normalized gain at both 391 and 428 nm as a function of pump ellipticity at a delay of ~ 0.45 ps and pump intensity of $\sim 4.5 \times 10^{14} \text{ W cm}^{-2}$. Integrated high harmonic intensity (H11-H21) is also shown as a function of pump ellipticity.

gain at 391 nm using this pump intensity and linear polarization. Gain is available for all pump ellipticities, including circular, for both lines. The overall shape of the ellipticity dependence of gain at 391 nm depends on pump pulse and gas jet parameters (see Figure 4(b) and (c)), as does the time-dependence, but gain using a circularly polarized pump was observed at intensities down to $\sim 9 \times 10^{13} \text{ W cm}^{-2}$ despite the short gain length.

These results contrast with high harmonic generation, which has a sharp ellipticity dependence for atoms and simple molecules like N_2 . Increasing ellipticity first reduces and then eliminates recollision. As a result, there

is a rapid decrease in harmonic efficiency with ellipticity [37]. To demonstrate this under conditions identical to that of the gain studied in Figure 4(c), we generate harmonics in the focus of the pump beam and measure their intensity using an in-line XUV spectrometer, which also allows us to calibrate the pump intensity using the high harmonic cut-off law. The intensity of the harmonics (H11-H21) as a function of ellipticity is also shown on Figure 4(c). Ellipticity of ~ 0.15 strongly reduces harmonic emission, but there is no indication of a sharp reduction to the N_2^+ gain. There is only one way to interpret Figure 4(c). Recollision does not contribute significantly to establishing the gain. Other mechanisms must be responsible.

In conclusion, we note that strong-field atomic, molecular, and optical physics experiments show that multiphoton ionization has three mechanisms for populating excited states of the ion. First, during ionization, both the ground and excited states can be directly populated [38–40]. Studies of D_2 [39] and HCl [38] indicate that this direct population can be on the order of a few percent depending on the energy level separation. While there is no quantitative experiment, nor theory, for N_2 ionization, high harmonics experiments demonstrate that some population is directly transferred to the $\text{B}^2\Sigma_u^+$ state upon strong field ionization of N_2 [41]. The total population transfer to the excited state of N_2^+ during ionization could exceed 17% by extrapolating the predicted excitation rates for D_2 ionization [39].

Inelastic scattering due to recollision is the second established mechanism [42]. We have shown that this does not contribute in the case of N_2^+ . A third mechanism is direct population of Rydberg states which rapidly recombine [43, 44]. The rapid rise and slow decay of the gain [15, 35, 36] seems to argue against this mechanism.

Finally, we note that population transfer can occur between electronic levels during the interaction of the newly created ion with the remainder of the pump pulse [45, 46]. This mechanism does not contribute to recollision. However, the experimental procedure that we have introduced of using short gas jets to isolate gain from filamentation will allow us to test the importance of the post ionization part of the pulse by tuning the pump pulse intensity, duration, or frequency, and will be a valuable tool for understanding the gain.

Acknowledgements: This work has benefited from stimulating discussion with Michael Spanner, Andr  Myszrowicz, Yi Liu, Pavel Polynkin, Misha Ivanov and Andrius Baltu ka. We would like to especially point out the contribution of Michael, who was the first person to argue that recollision did not play a role in N_2^+ gain, a conclusion arrived at based on his unpublished computations. We also appreciate the engineering expertise of Tyler Clancy

This research is supported by the US Army Research Office through an award number W911NF-14-1-0383 as

well as Canada's National Research Council, and the National Science and Engineering Research Council of Canada.

* Mathew.Britton@uOttawa.ca

- [1] A. Braun, G. Korn, X. Liu, D. Du, J. Squier, and G. Mourou, *Opt. Lett.* **20**, 73 (1995).
- [2] S. L. Chin, *Femtosecond Laser Filamentation*, edited by S. L. Chin (Springer-Verlag New York, 2010).
- [3] A. Couairon and A. Mysyrowicz, *Physics Reports* **441**, 47 (2007).
- [4] S. Xu, J. Bernhardt, M. Sharifi, W. Liu, and S. L. Chin, *Laser Physics* **22**, 195 (2012).
- [5] D. Kartashov, S. Ališauskas, G. Andriukaitis, A. Pugžlys, M. Shneider, A. Zheltikov, S. L. Chin, and A. Baltuška, *Phys. Rev. A* **86**, 033831 (2012).
- [6] D. Kartashov, S. Ališauskas, A. Baltuška, A. Schmitt-Sody, W. Roach, and P. Polynkin, *Phys. Rev. A* **88**, 041805 (2013).
- [7] S. Mitryukovskiy, Y. Liu, P. Ding, A. Houard, and A. Mysyrowicz, *Opt. Express* **22**, 12750 (2014).
- [8] P. Ding, S. Mitryukovskiy, A. Houard, E. Oliva, A. Couairon, A. Mysyrowicz, and Y. Liu, *Opt. Express* **22**, 29964 (2014).
- [9] D. Kartashov, S. Ališauskas, A. Pugžlys, M. N. Shneider, and A. Baltuška, *Journal of Physics B: Atomic, Molecular and Optical Physics* **48**, 094016 (2015).
- [10] S. Mitryukovskiy, Y. Liu, P. Ding, A. Houard, A. Couairon, and A. Mysyrowicz, *Phys. Rev. Lett.* **114**, 063003 (2015).
- [11] J. Yao, B. Zeng, H. Xu, G. Li, W. Chu, J. Ni, H. Zhang, S. L. Chin, Y. Cheng, and Z. Xu, *Phys. Rev. A* **84**, 051802 (2011).
- [12] Y. Liu, Y. Brelet, G. Point, A. Houard, and A. Mysyrowicz, *Opt. Express* **21**, 22791 (2013).
- [13] W. Chu, G. Li, H. Xie, J. Ni, J. Yao, B. Zeng, H. Zhang, C. Jing, H. Xu, Y. Cheng, and Z. Xu, *Laser Physics Letters* **11**, 015301 (2014).
- [14] G. Li, C. Jing, B. Zeng, H. Xie, J. Yao, W. Chu, J. Ni, H. Zhang, H. Xu, Y. Cheng, and Z. Xu, *Phys. Rev. A* **89**, 033833 (2014).
- [15] Y. Liu, P. Ding, G. Lambert, A. Houard, V. Tikhonchuk, and A. Mysyrowicz, *Phys. Rev. Lett.* **115**, 133203 (2015).
- [16] H. Xu, E. Ltstedt, A. Iwasaki, and K. Yamanouchi, *Nature Communications* **6**, 8347 (2015).
- [17] J. Yao, S. Jiang, W. Chu, B. Zeng, C. Wu, R. Lu, Z. Li, H. Xie, G. Li, C. Yu, Z. Wang, H. Jiang, Q. Gong, and Y. Cheng, *Phys. Rev. Lett.* **116**, 143007 (2016).
- [18] C. Hauri, W. Kornelis, F. Helbing, A. Heinrich, A. Couairon, A. Mysyrowicz, J. Biegert, and U. Keller, *Applied Physics B* **79**, 673 (2004).
- [19] S. Akturk, A. Couairon, M. Franco, and A. Mysyrowicz, *Opt. Express* **16**, 17626 (2008).
- [20] Y. Liu, Q. Wen, S. Xu, W. Liu, and S. L. Chin, *Applied Physics B* **105**, 825 (2011).
- [21] C. C. Wang, *Physical Review* **152**, 149 (1966).
- [22] J. P. Palastro, *Phys. Rev. A* **89**, 013804 (2014).
- [23] O. Nagy, C. P. Ballance, K. A. Berrington, P. G. Burke, and B. M. McLaughlin, *Journal of Physics B: Atomic, Molecular and Optical Physics* **32**, L469 (1999).
- [24] P. B. Corkum, *Phys. Rev. Lett.* **71**, 1994 (1993).
- [25] C. Guo and G. N. Gibson, *Phys. Rev. A* **63**, 040701 (2001).
- [26] Z. Chang, in *Fundamentals of Attosecond Optics* (CRC Press, 2010) pp. 165–221.
- [27] P. Dietrich, N. H. Burnett, M. Ivanov, and P. B. Corkum, *Phys. Rev. A* **50**, R3585 (1994).
- [28] T. Brabec, M. Y. Ivanov, and P. B. Corkum, *Phys. Rev. A* **54**, R2551 (1996).
- [29] G. L. Yudin and M. Y. Ivanov, *Phys. Rev. A* **63**, 033404 (2001).
- [30] H. Zhang, C. Jing, G. Li, H. Xie, J. Yao, B. Zeng, W. Chu, J. Ni, H. Xu, and Y. Cheng, *Phys. Rev. A* **88**, 063417 (2013).
- [31] S. Rostami, J.-C. Diels, and L. Arissian, *Opt. Express* **23**, 3299 (2015).
- [32] S. Rostami, M. Chini, K. Lim, J. P. Palastro, M. Durand, J.-C. Diels, L. Arissian, M. Baudelet, and M. Richardson, *Scientific Reports* **6**, 20363 (2016).
- [33] K. Lim, M. Durand, M. Baudelet, and M. Richardson, *Scientific Reports* **4**, 7217 (2014).
- [34] C. T. L. Smeenk, L. Arissian, A. V. Sokolov, M. Spanner, K. F. Lee, A. Staudte, D. M. Villeneuve, and P. B. Corkum, *Phys. Rev. Lett.* **112**, 253001 (2014).
- [35] H. Zhang, C. Jing, J. Yao, G. Li, B. Zeng, W. Chu, J. Ni, H. Xie, H. Xu, S. L. Chin, K. Yamanouchi, Y. Cheng, and Z. Xu, *Phys. Rev. X* **3**, 041009 (2013).
- [36] M. Lei, C. Wu, A. Zhang, Q. Gong, and H. Jiang, *Opt. Express* **25**, 4535 (2017).
- [37] B. Shan, S. Ghimire, and Z. Chang, *Phys. Rev. A* **69**, 021404 (2004).
- [38] H. Akagi, T. Otobe, A. Staudte, A. Shiner, F. Turner, R. Dörner, D. M. Villeneuve, and P. B. Corkum, *Science* **325**, 1364 (2009).
- [39] I. V. Litvinyuk, F. Légaré, P. W. Dooley, D. M. Villeneuve, P. B. Corkum, J. Zanghellini, A. Pegarkov, C. Fabian, and T. Brabec, *Phys. Rev. Lett.* **94**, 033003 (2005).
- [40] S. Erattupuzha, S. Larimian, A. Baltuška, X. Xie, and M. Kitzler, *The Journal of Chemical Physics* **144**, 024306 (2016).
- [41] B. K. McFarland, J. P. Farrell, P. H. Bucksbaum, and M. Gühr, *Science* **322**, 1232 (2008).
- [42] M. F. Kling, C. Siedschlag, A. J. Verhoef, J. I. Khan, M. Schultze, T. Uphues, Y. Ni, M. Uiberacker, M. Drescher, F. Krausz, and M. J. J. Vrakking, *Science* **312**, 246 (2006).
- [43] N. H. Burnett and P. B. Corkum, *J. Opt. Soc. Am. B* **6**, 1195 (1989).
- [44] U. Eichmann, T. Nubbemeyer, H. Rottke, and W. Sandner, *Nature* **461**, 1261 (2009).
- [45] M. Sindelka, N. Moiseyev, and L. S. Cederbaum, *Journal of Physics B: Atomic, Molecular and Optical Physics* **44**, 045603 (2011).
- [46] G. J. Halász, A. Vibók, and L. S. Cederbaum, *The Journal of Physical Chemistry Letters* **6**, 348 (2015), pMID: 26261946.